Modeling of Solute Redistribution in the Mushy Zone during Solidification of Aluminum-Copper Alloys

Q.Z. DIAO and H.L. TSAI

A mathematical model has been established to predict the formation of macrosegregation for a unidirectional solidification of aluminum-copper alloys cooled from the bottom. The model, based on the continuum formulation, allows the calculation of transient distributions of temperature, velocity, and species in the solidifying alloy caused by thermosolutal convection and shrinkage-induced fluid flow. Positive segregation in the casting near the bottom (inverse segregation) is found, which is accompanied by a moving negative-segregated mushy zone. The effects of shrinkage-induced fluid flow and solute diffusion on the formation of macrosegregation are examined. It is found that the redistribution of solute in the solidifying alloy is caused by the flow of solute-rich liquid in the mushy zone due to solidification shrinkage. A higher heat-extraction rate at the bottom increases the solidification rate, decreasing the size of the mushy zone, reducing the flow of solute-rich liquid in the mushy zone and, as a result, lessening the severity of inverse segregation. Comparisons between the theoretical predictions from the present study and previous modeling results and available experimental data are made, and good agreements are obtained.

I. INTRODUCTION

SOLIDIFICATION of alloys is characterized by the existence of a mushy zone, in which the solid phase and liquid phase coexist. It has been reported that transport phenomena (*i.e.*, heat and mass transfer and fluid flow) in the mushy zone are the major cause for the formation of casting defects, such as segregation, porosity, and hot tears.[1,2] In particular, the formation of macrosegregation (*i.e.*, a large-scale nonuniformity in composition) in castings is understood to be caused by two mechanisms occurring in the mushy zone.[1] The first mechanism corresponds to the floating or settling of precipitated phases during solidification. The precipitated phases could be the equiaxed grains and/or broken dendrites in the mushy zone. The other mechanism is related to the flow of solute-rich or solute-poor liquid in the mushy zone. The fluid flow can be caused by solidification contraction and/or thermal and/or solutal gradients. A higher concentration of solute is frequently found near the bottom surface of a casting unidirectionally solidified from the bottom, which is commonly called inverse segregation. Inverse segregation is a kind of macrosegregation that has been reported to be caused by solidification contraction.[1]

In the past, many experimental and theoretical studies on the formation of inverse segregation have been reported. Scheil[3] developed an expression which can predict the "maximum segregation" at the chill surface as a function of alloy composition in a unidirectionally solidified ingot. Kirkaldy and Youdelis[4] extended Scheil's equation to predict not only the maximum segregation but the positional variation of the segregation. Their model, however, is limited to one dimension, and the momentum, energy, and species equations are not completely coupled. Perhaps the first rigorous model to predict the formation of macrosegregation was described in the pioneering articles by Flemings and co-workers.[5,6,7] The well known "local solute redistribution equation" was derived, which predicted successfully the formation of inverse segregation, centerline segregation, and segregation resulting from changes of cross section for unidirectional solidification of Al-Cu alloys. However, the solute diffusion was neglected, and the thermal gradients and velocity distributions used in the equation were measured or assumed.

Kato and Cahoon[8] studied the inverse segregation in directionally solidified Al-Cu-Ti alloys with equiaxed grains based on the theory proposed by Kirkaldy and Youdelis and reported that the theoretical predictions were consistent with the experimental measurements. Ohnaka and Matsumoto[9,10] have analyzed the unidirectional solidification of Al-Cu alloys based on the conservation of momentum, energy, and species and have incorporated the solute diffusion effects. However, they did not show the transient solute distribution, and the importance of shrinkage-induced flow on the formation of macrosegregation was not discussed.

Recently, Bennon and Incropera[11,12] and Beckermann and Viskanta[13] developed the "continuum formulation" based on the classical mixing theory or volume averaging technique, which is valid for the entire casting domain, including the solid phase, mushy zone, and liquid phase. Employing the continuum formulation, many multidimensional solidification problems involving a complete coupling of momentum, energy, and species equations have been solved. Neilson and Incropera[14] used the continuum formulation to study the unidirectional solidification of aqueous NH_4Cl and the effects of the compositionally-induced fluid motion. As aqueous NH_4Cl liquid in the mushy zone is enriched by the lighter H_2O species when solid NH_4Cl is precipitated, a density inversion is created, leading to pronounced freckle phenomena.[14] In the above-mentioned continuum

Q.Z. DIAO, Graduate Student, and H.L. TSAI, Associate Professor of Mechanical Engineering, are with the Department of Mechanical and Aerospace Engineering and Engineering Mechanics, University of Missouri–Rolla, Rolla, MO 65401.

Manuscripts submitted September 17, 1992.

formulation, with the exception of the buoyancy terms, a constant density was assumed throughout the entire domain, and as a result, the shrinkage effect was neglected.

For unidirectional solidification of Al-Cu alloys cooled from the bottom, as the heavier copper species is rejected when the solid aluminum is precipitated, stable solute and temperature gradients are created, and no natural convection can be induced. Hence, the inverse segregation in directionally solidified Al-Cu alloys cannot be predicted by the above-mentioned models. Chiang and Tsai[15,16] have modified the continuum formulation to include the fluid flow and domain change caused by solidification contraction. In their study, they concluded that shrinkage-induced fluid flow is dominated in the mushy zone compared with the natural convection due to temperature gradients. As the fluid flow in the mushy zone is the major cause of the formation of macrosegregation, the model will be extended in the present study to include the species equation to investigate the solute redistribution in the mushy zone during unidirectional solidification of Al-Cu alloys cooled from the bottom.

II. MATHEMATICAL FORMULATION

The model, based on the continuum formulation including the effect of shrinkage developed by Chiang and Tsai,[15,16] is used in the present study. In the derivation of the governing equations, the following assumptions are made: (1) the properties of the solid and liquid phases are homogeneous and isotropic; (2) the solid and liquid phases in the mushy zone are in local thermodynamic equilibrium; (3) the density for each phase is constant but can be different for the liquid and solid phases; (4) the Boussinesq approximation for natural convection can be invoked; (5) no pore formation is present; and (6) binary alloys. Based on the continuum formulation, the continuity, momentum, energy, and species equations for the solidification of a two-dimensional casting are given as follows:

Continuity

$$\frac{\partial}{\partial t}(\rho) + \nabla \cdot (\rho \mathbf{V}) = 0 \qquad [1]$$

where t is the time, ρ is the density, and $\mathbf{V}$ is the velocity vector.

Momentum

$$\frac{\partial}{\partial t}(\rho u) + \nabla \cdot (\rho \mathbf{V} u) = \nabla \cdot \left(\mu_l \frac{\rho}{\rho_l} \nabla u \right) - \frac{\partial p}{\partial x} - \frac{\mu_l}{K} \frac{\rho}{\rho_l} (u - u_s) - \frac{C\rho^2}{K^{1/2}\rho_l} |u - u_s| (u - u_s) - \nabla \cdot (\rho f_s f_l \mathbf{V}_r u_r) + \nabla \cdot \left(\mu_l u \nabla \left(\frac{\rho}{\rho_l} \right) \right) \qquad [2]$$

$$\frac{\partial}{\partial t}(\rho v) + \nabla \cdot (\rho \mathbf{V} v) = \nabla \cdot \left(\mu_l \frac{\rho}{\rho_l} \nabla v \right) - \frac{\partial p}{\partial y} - \frac{\mu_l}{K} \frac{\rho}{\rho_l} (v - v_s) - \frac{C\rho^2}{K^{1/2}\rho_l} |v - v_s| (v - v_s) - \nabla \cdot (\rho f_s f_l \mathbf{V}_r v_r) + \nabla \cdot \left(\mu_l v \nabla \left(\frac{\rho}{\rho_l} \right) \right) + \rho g (\beta_T (T - T_0) + \beta_s (f_l^\alpha - f_{l,0}^\alpha)) \qquad [3]$$

where u and v are the velocities in the x- and y-directions, respectively, and $\mathbf{V}_r$ ($= \mathbf{V}_l - \mathbf{V}_s$) is the relative velocity vector between the liquid phase and the solid phase. The subscripts s and l refer to the solid and liquid phases, respectively; p is the pressure; μ is the viscosity; f is the mass fraction; K, the permeability function of the casting, is a measure of the ease with which fluids pass through the porous mushy zone; C is the inertial coefficient; β_T and β_s are the thermal expansion coefficient and solutal expansion coefficient, respectively; g is gravitational acceleration; and T is the casting temperature. The subscript 0 represents initial condition, and the superscript α represents species. The third and fourth terms on the right-hand side of Eqs. [2] and [3] represent the first- and second-order drag forces, respectively, for the flow in the mushy zone. The second-to-last term on the right-hand side of Eq. [2] and the third term from the last on the right-hand side of Eq. [3] represent an interaction between the solid and the liquid phases. These two terms are zero except in the mushy zone, in which case neither f_s nor f_l is zero. The last term on the right-hand side of Eq. [2] and the second-to-last term on the right-hand side of Eq. [3] represent the effect of shrinkage, and both terms are identical to zero when the density difference between the solid and liquid phases is not considered. The last term on the right-hand side of Eq. [3] is based on the Boussinesq approximation for natural convection. It is noted that Eqs. [2] and [3] reduce to appropriate single-phase limits (*i.e.*, K is zero in the pure solid and K is infinite in the pure liquid, see also Eq. [8]).

Energy

$$\frac{\partial}{\partial t}(\rho h) + \nabla \cdot (\rho \mathbf{V} h) = \nabla \cdot \left(\frac{k}{c_s} \nabla h \right) + \nabla \cdot \left(\frac{k}{c_s} \nabla (h_s - h) \right) - \nabla \cdot (\rho (\mathbf{V} - \mathbf{V}_s) (h_l - h)) \qquad [4]$$

where h is the enthalpy, k is the thermal conductivity, and c is the specific heat. The first two terms on the right-hand side of Eq. [4] represent the net Fourier diffusion flux. The last term represents the energy flux associated with the relative phase motion.

Species

$$\frac{\partial}{\partial t}(\rho f^{\alpha}) + \nabla\cdot(\rho \mathbf{V} f^{\alpha}) = \nabla\cdot(\rho D \nabla f^{\alpha}) + \nabla\cdot(\rho D \nabla(f_l^{\alpha} - f^{\alpha})) - \nabla\cdot(\rho(\mathbf{V} - \mathbf{V}_s)(f_l^{\alpha} - f^{\alpha})) \quad [5]$$

where D is the mass diffusion coefficient. The first two terms on the right-hand side of Eq. [5] represent the net Fickian diffusion flux, while the last term represents the species flux due to relative phase motion. In Eqs. [1] through [5], the continuum density, specific heat, thermal conductivity, mass diffusivity, solid mass fraction, liquid mass fraction, velocity, enthalpy, and mass fraction of constituent α are defined as follows:

$$\rho = g_s\rho_s + g_l\rho_l; \qquad c = f_s c_s + f_l c_l; \qquad k = g_s k_s + g_l k_l$$

$$D = f_s D_s + f_l D_l; \qquad f_s = \frac{g_s\rho_s}{\rho}; \qquad f_l = \frac{g_l\rho_l}{\rho}$$

$$\mathbf{V} = f_s\mathbf{V}_s + f_l\mathbf{V}_l; \qquad h = f_s h_s + f_l h_l; \qquad f^{\alpha} = f_s f_s^{\alpha} + f_l f_l^{\alpha} \quad [6]$$

where g_s and g_l are the volume fractions of the solid and liquid phases, respectively.

If the phase specific heats are assumed constant, the phase enthalpy for the solid and liquid can be expressed as

$$h_s = c_s T; \qquad h_l = c_l T + (c_s - c_l)T_e + H \quad [7]$$

where H is the latent heat of the alloy and T_e is the eutectic temperature.

The assumption of permeability function in the mushy zone requires consideration of the growth morphology specific to the alloy under study. In the present study, the permeability function analogous to fluid flow in the porous media is assumed, employing the Carman-Kozeny equation[17,18]

$$K = \frac{g_l^3}{c_1(1 - g_l)^2}; \qquad c_1 = \frac{180}{d^2} \quad [8]$$

where d is proportional to the dendrite dimension, which is assumed to be a constant and is on the order of 10^{-2} cm. The inertial coefficient, C, can be calculated from[19]

$$C = 0.13 g_l^{-3/2} \quad [9]$$

Closure of the system of conservation equations requires supplementary relations. With the assumption of local thermodynamic equilibrium, the required relations may be obtained from the equilibrium phase diagram. Neglecting the curvatures in the solidus and liquidus lines in the phase diagram, the solid mass fraction and solid- and liquid-phase compositions can be expressed as

$$f_s = \frac{1}{1 - k_p}\left[\frac{T - T_l}{T - T_m}\right]; \qquad f_s^{\alpha} = \left[\frac{k_p}{1 + f_s(k_p - 1)}\right] f^{\alpha};$$

$$f_l^{\alpha} = \left[\frac{1}{1 + f_s(k_p - 1)}\right] f^{\alpha} \quad [10]$$

where T_l is the liquidus temperature corresponding to f^{α}, T_m is the fusion temperature when $f^{\alpha} = 0$, and the equilibrium partition ratio k_p is the ratio of the slopes for the liquidus and solidus lines. It is noted that the assumption of local equilibrium does not preclude the existence of a nonequilibrium condition on a macroscopic scale.

In the previous governing differential equations (Eqs. [1] through [5]), there is a solid-phase velocity. The solid-phase velocity is associated with the movement of precipitated solid equiaxed grains and/or broken dendrites in the mushy zone. Generally, there are certain relations between the solid-phase and liquid-phase velocities;[20] however, the exact relations are not known at this time. Also, under the condition of unidirectional solidification cooled from the bottom, the solid phase is likely to be stationary. Hence, we assume the solid-phase velocity is zero in the present study, and the equations are simplified accordingly.

III. NUMERICAL METHOD

The governing equations are in the general format, as suggested by Patankar,[21] for the numerical solution of heat and fluid flow problems (*i.e.*, they contain a transient term, a diffusion term, a convection term, and source terms). Hence, any established numerical procedure for solving coupled elliptic partial differential equations can be used, with slight modifications for the source terms. In the present study, the equations were solved iteratively at each time step using the control-volume-based finite difference procedure described by Patankar.[21] A fully implicit formulation was used for the time-dependent terms, and the combined convection/diffusion coefficients were evaluated using an upwind scheme. The SIMPLEC algorithm was applied to solve the momentum and continuity equations to obtain the velocity field. At each time step, the momentum equations were solved first in the iteration process using the most updated volume fractions of solid and liquid for the mixture density, the permeability function, and the mass fractions of solid and liquid. Then, the energy equation was solved to obtain enthalpy, with which the temperature can be calculated. Similarly, the species equation was solved to obtain the concentration distribution. Next, the volume fractions of solid and liquid, the permeability, and the mass fractions of solid and liquid can be updated. This process was repeated for each iteration step. For each time step, iterations were terminated when the maximum residual source of mass, momentum, energy, and species was less than 1×10^{-5}. A line-by-line solver, based on the tridiagonal matrix algorithm (TDMA), was used to solve iteratively the algebraic discretization equations. The last five terms on the right-hand side of Eq. [2], the last six terms on the right-hand side of Eq. [3], and the last two terms on the right-hand side of Eqs. [4] and [5] represent the source terms and are treated according to the procedure suggested by Patankar.[21] More details about the computational procedure used in the present study can be found in the previous articles.[15,16]

As the governing equations are valid in the pure liquid and solid regions and the mushy zone, there is no need to track the geometrical shape and the extent of each

region. Hence, a fixed-grid system was used in the numerical calculation. Figure 1 shows the grid system of the casting domain. A grid system of 46 × 61 points was utilized for the casting domain of 4 × 20 cm. Due to the symmetry of the domain, only half of the grid points (*i.e.*, 23 × 61) were used in the actual calculation. The grid was slightly skewed to provide a higher concentration of nodal points near the bottom of the casting, where larger temperature and solutal gradients were present. A finer grid system will certainly give more accurate computational results, but the CPU time needed for the computation will also be increased. Hence, the mesh size used in the present work is a compromise between the accuracy and the computational cost. During solidification, due to density change, the total casting domain decreases with time. The domain change is handled by the front tracking method, and a detailed description can be found in previous publications.[15,16] It is noted that the numerical method used in the present study has been extensively tested by the authors in many other problems.[22] Hence, the results obtained from the present study should be reliable. A variable time-step size is used in the calculation to provide optimum solution accuracy while maintaining numerical stability. The initial time-step size is 0.0001 seconds, and the maximum time-step size is 0.025 seconds. The calculations were executed on Apollo DN10000 and HP*-730 workstations. Typical CPU time required for the calculation of each case is about 100 hours.

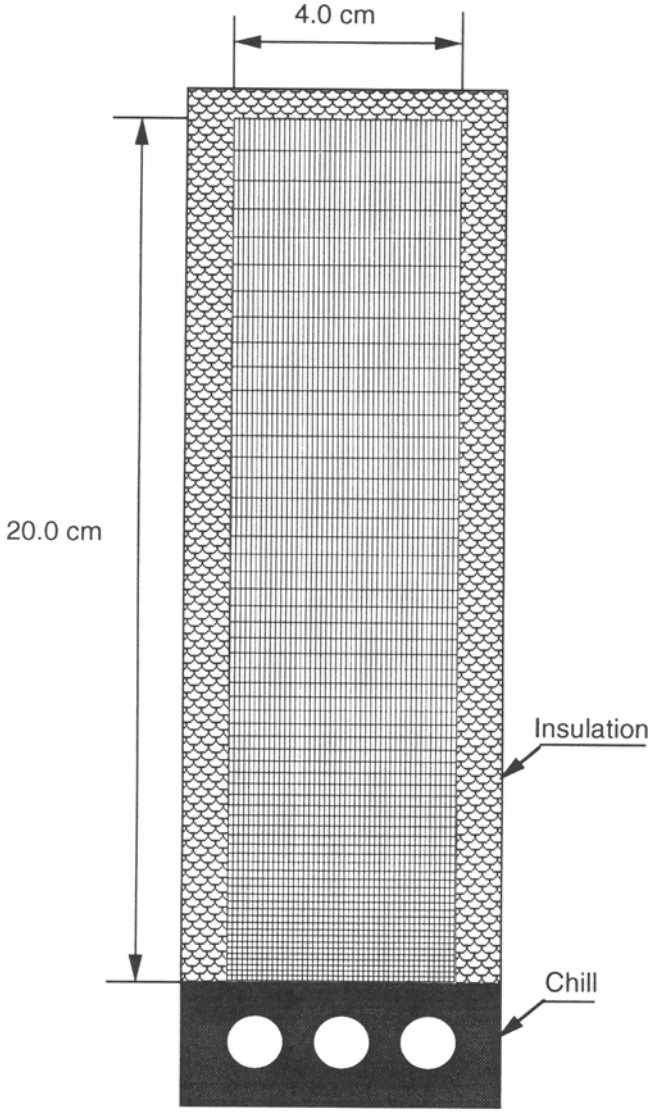

Fig. 1—Schematic representation of the physical domain and the mesh system.

*HP is a trademark of Hewlett-Packard Company, Colorado Springs, Co.

IV. RESULTS AND DISCUSSION

A. *Temperature, Velocity, and Solute Distributions*

As shown in Figure 1, a unidirectional solidification can be induced by passing some coolant at a desired temperature, T_c, through a chill placed at the bottom of the casting while the other sides of the casting are insulated. Heat transfer between the chill and the casting is accomplished *via* convection through an effective convective heat-transfer coefficient h_c. An A1-4.1 wt pct Cu alloy is used in the present study, and its thermophysical properties and the casting conditions are summarized in Table I.

As the casting will start to solidify from the bottom, there will be an upward positive temperature gradient in the casting. Hence, it is expected that a stable temperature field exists in the casting, and no natural convection due to inverse temperature gradients is present. Also, during alloy solidification, heavier copper species will be rejected starting from the bottom. Hence, it is expected that more copper species will be accumulated in the lower portion of the casting, creating a stable negative solutal gradient. In other words, neither temperature gradients nor solutal gradients will induce natural

Table I. Thermophysical Properties of Al-4.1 Pct Cu and Casting Conditions

Symbol	Value	Unit	Reference
c_s	1.0928	J $g^{-1}K^{-1}$	23
c_l	1.0588	J $g^{-1}K^{-1}$	23
D_l	3×10^{-5}	cm^2s^{-1}	assumed
D_s	≈0		assumed
k_s	1.9249	W $cm^{-1}K$	23
k_l	0.8261	W $cm^{-1}K$	23
k_p	0.170		23
ρ_s	2.65	g cm^{-3}	23
ρ_l	2.40	g cm^{-3}	23
β_T	4.95×10^{-5}	K^{-1}	assumed
β_s	−2.0		assumed
μ	0.03	g $cm^{-1}s^{-1}$	23
H	397.5	J g^{-1}	23
T_e	821.2	K	23
T_m	933.2	K	23
$f_{l,0}^{\alpha}$	4.1	Pct	
T_0	970.0	K	
T_c	293.0	K	
h_c	0.02	W $cm^{-2}K^{-1}$	

convection in the casting. Hence, under the solidification conditions used in the present study, the only possible driving force for the fluid flow in the casting is solidification contraction.

Figure 2(a) shows the isotherms in the casting at a time of 180 seconds. As expected, all isotherms are planar, and the temperature increases upward. Corresponding temperature distribution along the vertical direction is given in Figure 2(b). The liquidus and solidus fronts are also shown in the figure, indicating the regions of solid phase, mushy zone, and liquid phase. The positions of the liquidus front and solidus front and the size of the mushy zone as functions of time are shown in Figure 3. It is seen that the size of the mushy zone increases with time as it moves away from the chill. Figure 4(a) shows the velocity distribution in the casting at a time of 180 seconds. As explained above, the fluid flow is caused only by solidification contraction; hence, the direction of the velocity is toward the chill. The length of the arrow in the figure represents the magnitude of the velocity. The velocity is generally small compared with typical values found in forced convection or natural convection. With the exception of the no-slip condition at the wall, the velocity in the mushy zone becomes nearly uniform in the horizontal direction, which is caused by the fact that an isotropic permeability function is assumed in the present study. It is noted that the velocity shown in the figure is the continuum velocity, as defined in Eq. [6], which is weighted by the liquid fraction (the solid-phase velocity is assumed to be zero in the present study). A more detailed velocity profile along the centerline of the casting is given in Figure 4(b). It is seen that the continuum velocity is constant in the pure liquid phase and decreases abruptly toward the chill in the mushy zone. However, the actual liquid-phase velocity remains very high in most portions of the mushy zone, compared to the continuum velocity in the pure liquid phase.

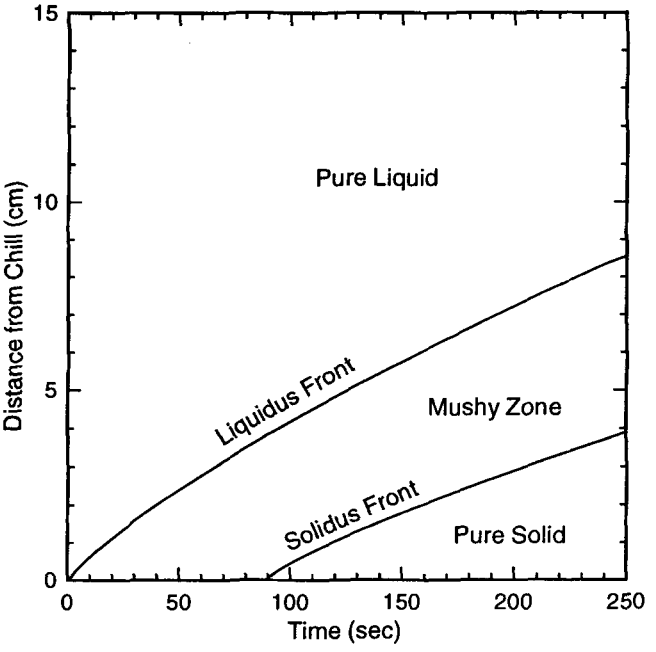

Fig. 3—Positions of the liquidus and solidus fronts as functions of time.

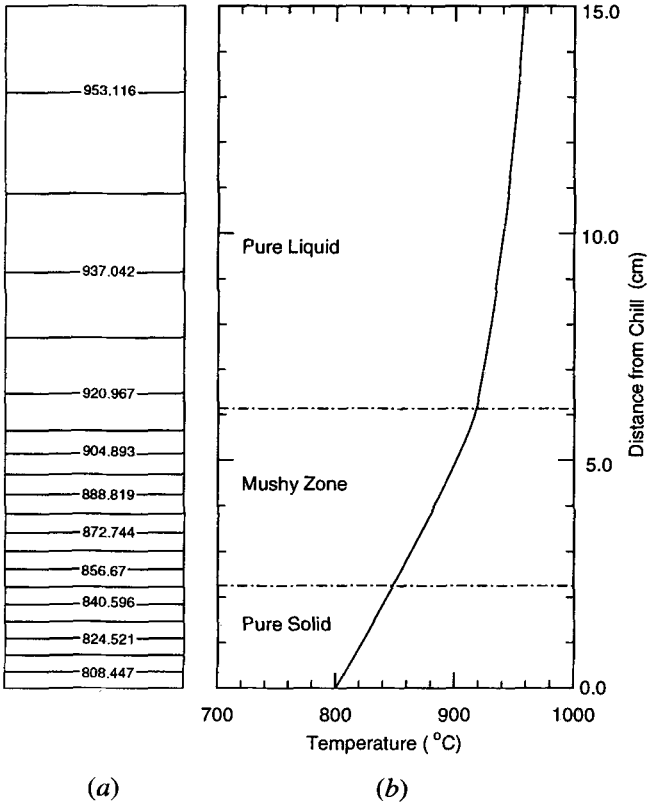

Fig. 2—(*a*) Isotherms: (*b*) temperature distribution along the vertical direction at t = 180 s.

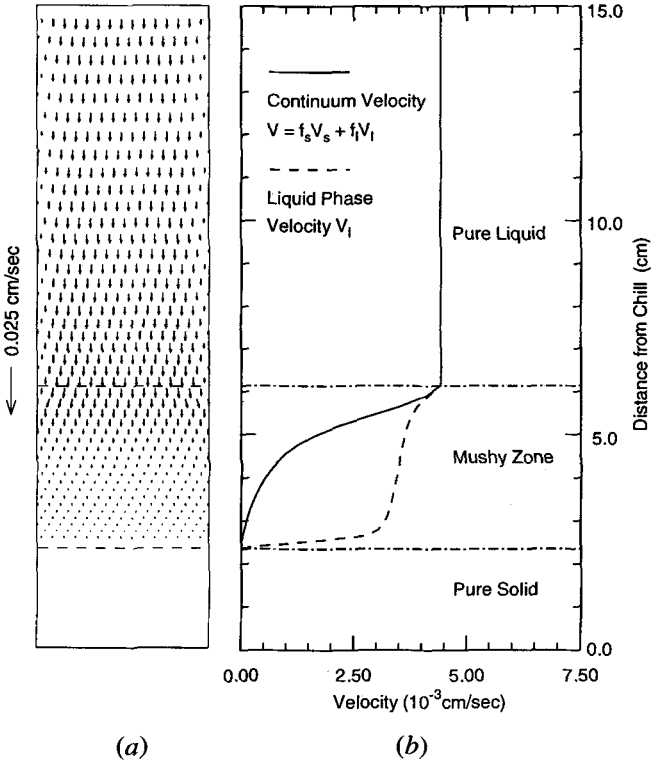

Fig. 4—(*a*) Velocity vectors: (*b*) velocity distribution along the centerline in the vertical direction at t = 180 s.

Figure 5(a) shows the isoconcentrations in the casting that are planar, similar to the isotherms. However, the copper concentration does not decrease monotonically from the bottom as the temperature field; instead, it decreases, up to some location in the mushy zone, to a minimum concentration lower than the initial value, and then increases to the initial copper concentration. The copper concentration along the vertical direction is shown in Figure 5(b), where it can be clearly seen that a positive-segregated (*i.e.*, above the initial copper concentration) region near the chill and a negative-segregated (*i.e.*, below the initial copper concentration) mushy zone are present. The higher copper concentration in the solidified casting near the chilled surface is commonly called inverse segregation. There is an abrupt change in solute concentration at both the solidus and liquidus fronts, and the copper concentration in the pure liquid phase remains the same as the initial value. Except in the region very near the solidus front, the copper concentration in the mushy zone is below the initial value. It is noted that the total solute accumulated in the positive-segregated region must be equal to the total solute depreciated in the negative-segregated region in order to satisfy the conservation of total solute. It is also noted that a positive solutal gradient exists between the location with minimum solute concentration in the mushy zone and the liquidus front. However, the positive solutal gradient is caused by the downward shrinkage-induced flow and, hence, cannot create natural convection. In fact, a negative solutal gradient exists for the liquid phase in the entire mushy zone, which will be discussed next.

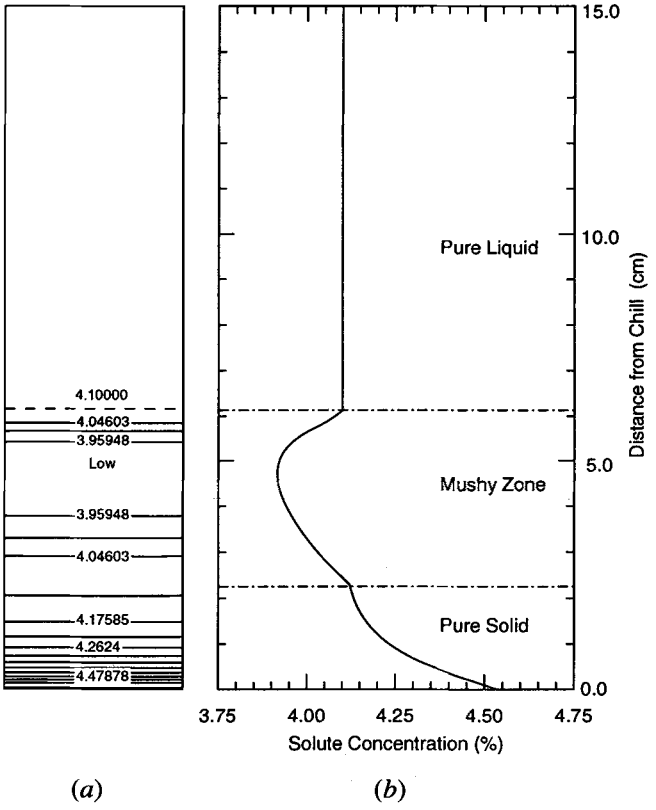

Fig. 5—(*a*) Isoconcentrations: (*b*) solute distribution along the vertical direction at t = 180 s.

In order to explain the phenomena observed in Figure 5(b), detailed solute distributions in the casting are given in Figure 6. In Figure 6(a), the local solute concentration in the solid phase, f_s^α, is defined as the mass fraction of solute in a unit mass of solid phase. Similarly, the local solute concentration in the liquid phase, f_l^α, is defined as the mass fraction of solute in a unit mass of liquid phase. During solidification, copper species is rejected into the liquid phase, and as a result, the local solute concentration of the liquid phase in the mushy zone increases continuously toward the chill, as shown in Figure 6(a). As the solute concentration of solid phase in the mushy zone is equal to the partition ratio times the solute concentration in the liquid phase, it also increases toward the chill. In the pure liquid region, f_l^α is constant, but in the pure solid region, f_s^α increases toward the chill. The corresponding solid fraction, f_s, and liquid fraction, f_l, in the casting, as defined in Eq. [6], are shown in Figure 6(b). The liquid fraction increases, starting from zero at the solidus front, to units at the liquidus front and beyond. Similarly, the solid fraction increases, starting from zero at the liquidus front, to units at the solidus front and toward the chill. The product $f_s f_s^\alpha$, the total amount of solute in the solid phase per

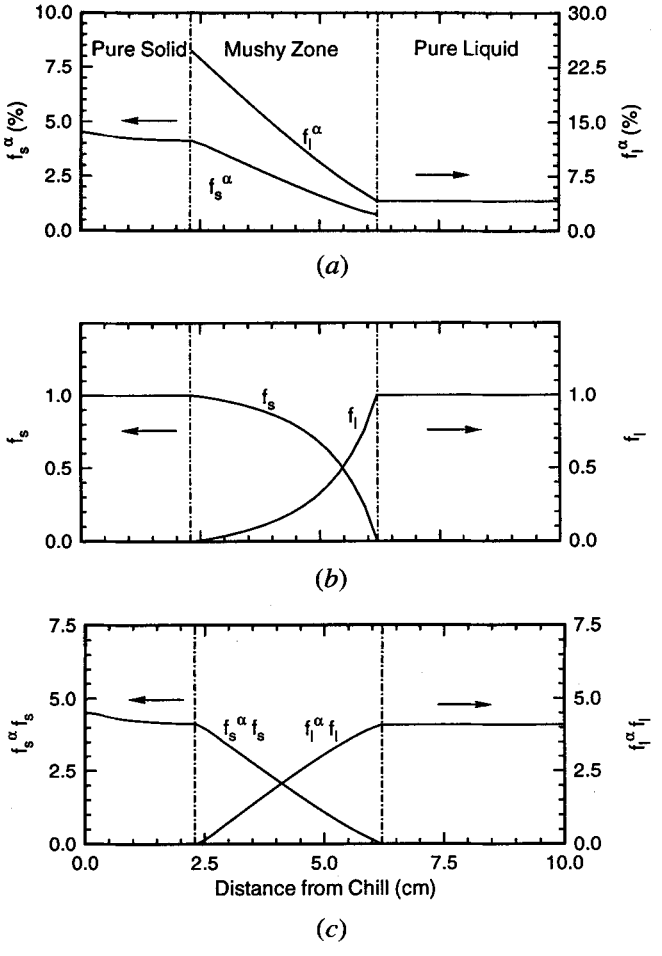

Fig. 6—(*a*) Local solute distributions in the solid and liquid phases: (*b*) distributions of solid and liquid fractions: (*c*) total solute in the solid and liquid phases, all at t = 180 s.

unit mass of mixture (liquid and solid mixture in the mushy zone), increases toward the chill. On the other hand, the product, $f_l f_l^\alpha$, the total amount of solute in the liquid phase per unit mass of alloy mixture, decreases toward the chill. The final solute concentration, f^α, as given in Eq. [6], is the sum of these two products, *i.e.*,

$$f^\alpha = f_s f_s^\alpha + f_l f_l^\alpha \quad [11]$$

which is plotted in Figure 5(b). Hence, from the above discussion, it is understood that the formation of a negative-segregated mushy zone is caused by the flow of solute-rich liquid in the mushy zone due to solidification contraction. However, near the chill at the bottom of the casting, the velocity of the fluid carrying solute slows down (and becomes zero at the wall), causing the solute to pile up, which leads to the inverse segregation in the casting.

Figure 7 shows a sequence of solute concentration profiles during solidification. The higher solute concentration in the region near the chill increases with time until the region is solidified, then the solute concentration in the solid phase remains unchanged, because the mass diffusion coefficient in the solid phase is negligible.

B. *Factors Affecting the Solute Distribution*

As the solid-phase velocity is assumed zero in the present study, solute redistribution in a solidifying casting can be caused only by fluid flow and diffusion mechanisms. If there is no fluid flow and no solute diffusion, the solute concentration should remain the same as the initial value. Since shrinkage-induced flow is the only possible flow for the unidirectional solidification considered in the present study, the effects of shrinkage-induced flow and solute diffusion on the solute redistribution are discussed in the following.

1. *If the shrinkage-induced flow is neglected*

The shrinkage effect can be neglected in the mathematical modeling by nullifying the corresponding terms in Eqs. [2] and [3] (*i.e.*, the last term and the second-to-last term on the right-hand side of Eq. [2] and Eq. [3], respectively). The density is constant throughout the casting, and the average value of the solid and liquid densities given in Table I is used in the modeling. Under this condition, there is no fluid flow in the alloy, and the solute redistribution is caused only by the diffusion mechanism. As the copper species will be rejected into the liquid phase during solidification, the solute concentration in the mushy zone is slightly higher than that in the pure solid phase, as shown in Figure 8. A maximum solute concentration occurs in the mushy zone near the liquidus front. However, the difference in solute distribution for the entire casting is relatively small compared with that in Figure 7, because the species diffusion is a very slow process, evidenced by a small value of mass diffusion coefficient given in Table I. It is noted that a slightly lower solute concentration in the pure solid phase and the lower portion of the mushy zone is compensated by the higher concentration in the upper portion of the mushy zone near the liquidus front, so that the overall conservation of copper species is satisfied.

2. *If the solute diffusion is neglected*

Solute diffusion in the casting can be neglected if the solute diffusion coefficient D in Eq. [5] is assumed to be zero. Under this condition, Figure 9 illustrates the solute distribution in the casting at a time of 180 seconds. By comparing Figure 5(b) with Figure 9, nearly identical solute distribution in the casting is found. This implies that under the conditions of the present study, the solute redistribution is controlled mainly by the fluid flow due to solidification shrinkage. The result is also consistent with the previous discussion concluding that the diffusion mechanism is not the primary factor contributing to the formation of macrosegregation. Hence, it is concluded that the formation of inverse segregation

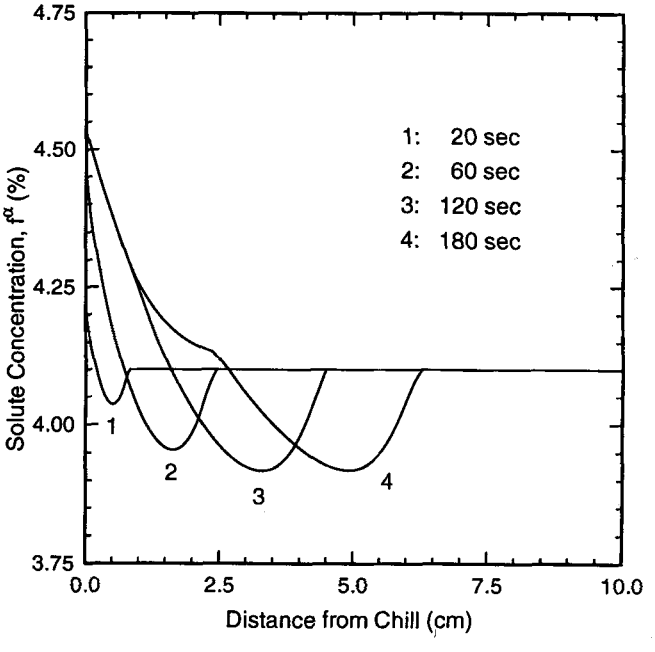

Fig. 7—Solute distribution at different times.

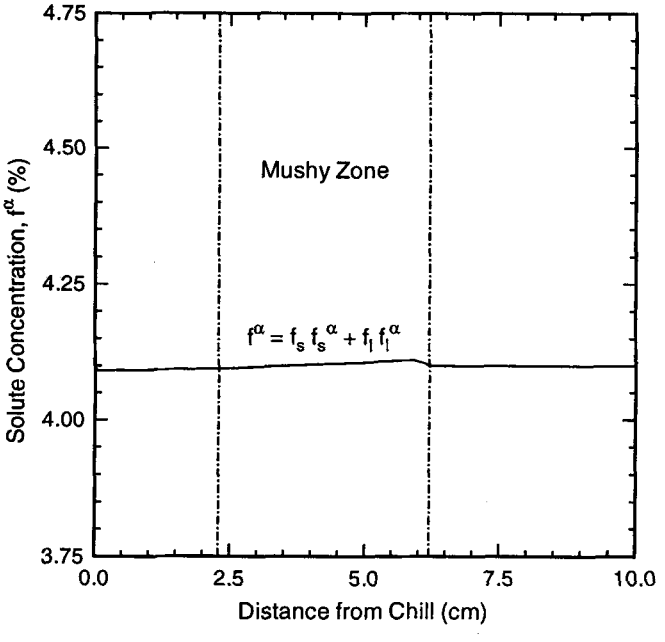

Fig. 8—Solute distribution when shrinkage-induced flow is neglected at t = 180 s.

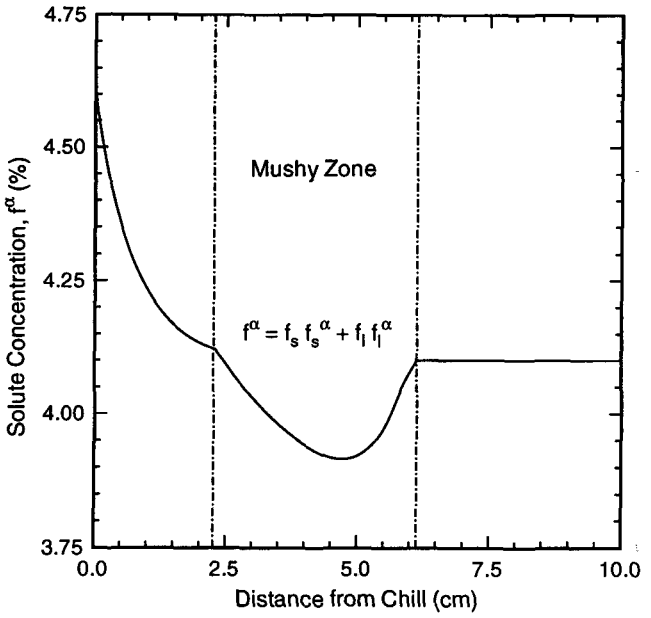

Fig. 9—Solute distribution when solute diffusion is neglected at t = 180 s.

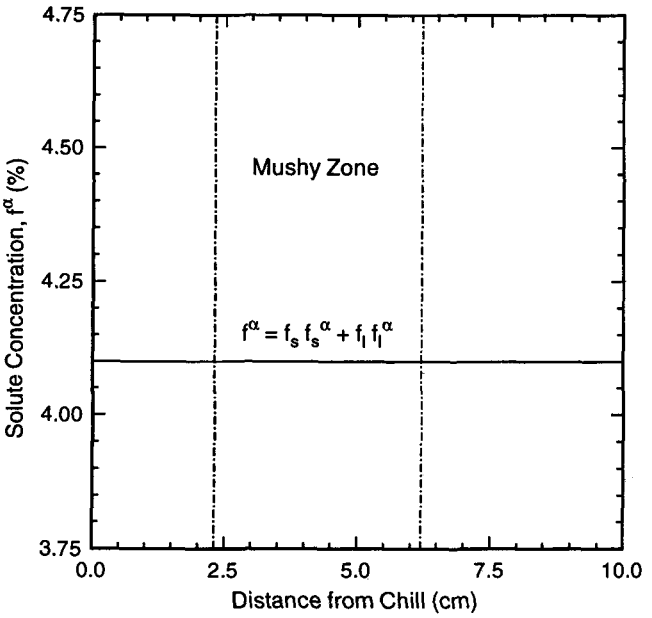

Fig. 10—Solute distribution when both shrinkage-induced flow and solute diffusion are neglected at t = 180 s.

near the bottom of the casting is caused by solidification contraction. It is noted that solute diffuses from locations of higher concentration to locations of lower concentration, while solute transportation by fluid flow depends on the direction of the fluid flow. In the present study, the fluid flow is caused only by shrinkage, and the solute-rich liquid flows toward the bottom of the casting. However, the solute diffuses upward from the higher concentration at the bottom of the casting. The net result is that the maximum segregation at the bottom of the casting in Figure 9 is slightly higher than that in Figure 5(b).

3. *If both the solute diffusion and shrinkage-induced flow are neglected*

In this case, both the solute diffusion coefficient in Eq. [5] and terms related to shrinkage effect in Eqs. [2] and [3] are set to zero. Under this condition, it is expected that there is no solute redistribution, and the solute concentration in the entire casting should be equal to the initial value.

Although microscopically the solute will be rejected from the solidifying dendrites or solid grains into the interdendritic liquid, there is no mechanism to transport the solute; hence, the average solute concentration (*i.e.*, from the macroscopic point of view) should remain the same as the initial value. Figure 10 shows the calculation result from the mathematical model proposed in the present study, which is as expected. In fact, the result shown in Figure 10 provides an excellent opportunity to test the correctness of the mathematical model and its associated numerical technique established in the present study, at least in the limiting case.

C. *Comparison with the Model by Flemings and Nereo*

For comparison, the "local solute redistribution equation" derived by Flemings and Nereo[5] is rewritten in the following:

$$\frac{\partial g_l}{\partial f_l^\alpha} = -\left(\frac{1-\beta}{1-k_p}\right)\left(1+\frac{\mathbf{V}\cdot\nabla T}{\varepsilon}\right)\frac{g_l}{f_l^\alpha} \qquad [12]$$

where β is the solidification contraction, ε is the rate of temperature change, and ∇T is the temperature gradient. Equation [12] was derived by combining the conservation of solute mass and the conservation of total mass. The solute diffusion was neglected in the derivation. It is noted that in order to use Eq. [12], the data regarding velocity distribution, temperature gradients, and the rate of temperature change must be obtained first. Flemings *et al.*[5,6,7] obtained the data through experimental measurements or by assumptions, and they used the equation to successfully predict the formation of inverse segregation and banding segregation. In the present study, the velocity and temperature distributions calculated from the momentum and energy equations (*i.e.*, Eqs. [1] through [4]) without considering the species caused the convection term in Eq. [3], and the species equation, Eq. [5], will be used to substitute into Eq. [12]. For convenience, the above equation is integrated to obtain the following form:

$$f_l^\alpha = f_{l,0}^\alpha \exp\left[-\left(\frac{1-k_p}{1-\beta}\right)\int_1^{g_l}\left(1+\frac{\mathbf{V}\cdot\nabla T}{\varepsilon}\right)^{-1}\frac{dg_l}{g_l}\right] \qquad [13]$$

Hence, the transient solute distribution in the casting can be obtained by substituting the transient velocity, temperature gradients, and the rate of temperature change calculated from Eqs. [1] through [4]. Figure 11 shows the solute distribution calculated by Eq. [13] and by the comprehensive model proposed in the present study at a time of 100 seconds. It is seen that good agreements between these two methods are obtained. The small difference could be caused by the neglecting of solute diffusion and the decoupling of the species equation from the momentum and energy equations in Eq. [13].

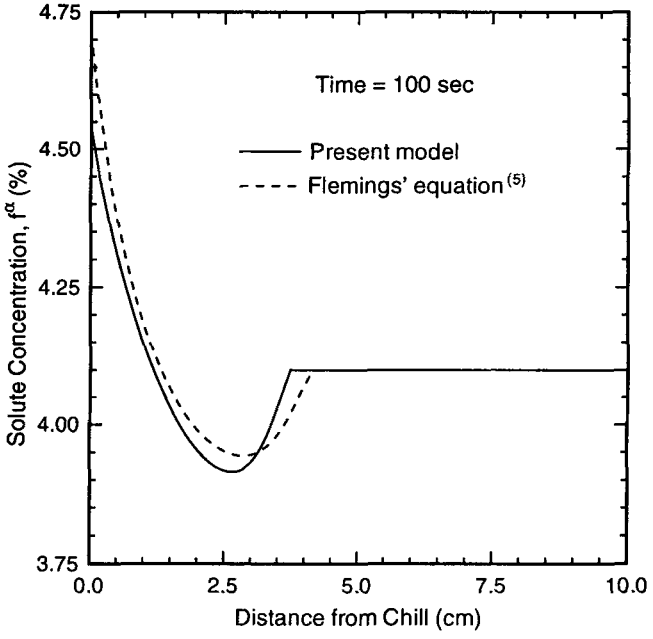

Fig. 11—Comparison between the present study and the results obtained from the "local solute redistribution equation" by Flemings and Nereo[5] at t = 100 s.

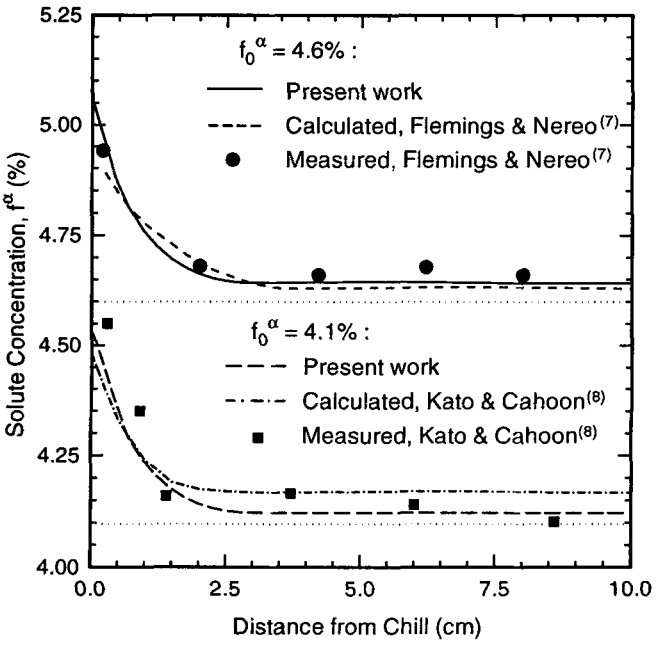

Fig. 12—Calculated results and experimental data for the solute distributions in the completely solidified castings.

D. *Final Solute Distribution in the Solidified Casting*

The final solute distribution after the casting is completely solidified is given in Figure 12. It is noted that only the solidified portion of the casting near the chill is plotted in the figure, and still a negative-segregated mushy zone exists at a distance further away from the chill. The experimental data and the calculated results of Flemings and Nereo[7] for 4.6 pct initial copper concentration and the results of Kato and Cahoon[8] for 4.1 pct initial copper concentration are also shown in the figure. It is seen that excellent agreements between the predictions of the present study and the results of previous studies are obtained. It is noted that the previous theoretical predictions are based on much simpler and restricted models, and they do not show the transient phenomena as the present model does. From Figure 12, it can be concluded that the mathematical model and its associated numerical technique established by the present study are appropriate. As the solid-phase velocity is assumed to be zero in the present study, it can also be said that under the unidirectional solidification cooled from the bottom, the assumption of a stationary solid phase is acceptable.

E. *Effect of Heat Extraction Rate on Inverse Segregation*

The effect of the heat extraction rate on the formation of inverse segregation can be studied by varying the convective heat-transfer coefficient between the chill and the casting. Figure 13 shows the inverse segregation for three different heat-transfer coefficients. It is seen that a higher heat-transfer coefficient increases the solidification rate and decreases the severity of inverse segregation. This is because a higher solidification rate decreases the size of the mushy zone, and the time required for solute-rich liquid in the mushy zone to flow "against" the chill is decreased. In other words, less solute can be carried by the fluid flow in the smaller mushy zone to pile up near the chill.

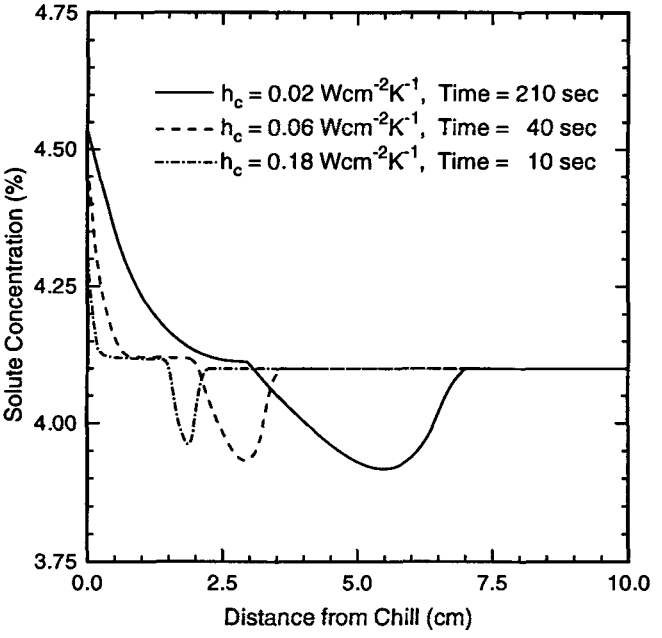

Fig. 13—Effect of heat-extraction rate at the bottom on the inverse segregation.

V. CONCLUSIONS

A numerical simulation of the formation of macrosegregation has been conducted for a unidirectional solidification of aluminum-copper alloys cooled from the

bottom. The mathematical model, based on the continuum formulation, allows a complete coupling between the momentum, energy, and species equations and a simple treatment of the casting domain, including the solid phase, mushy zone, and liquid phase. Natural convection due to temperature and solute gradients and shrinkage-induced fluid flow are considered in the present model. Transient temperature, velocity, and species distributions in the solidifying casting are calculated. The results from the present study indicate that the mathematical model and its associated numerical technique established in the present study can accurately predict the formation of inverse segregation. The major conclusions can be summarized as follows:

1. A positive segregation of species in the casting near the chill (inverse segregation) is predicted. This segregation is accompanied by a moving and negative-segregated mushy zone.
2. The formation of inverse segregation and negative-segregated mushy zone is caused by the fluid flow of solute-rich liquid in the mushy zone due to solidification contraction. The effect of shrinkage-induced flow on the solute redistribution in the mushy zone is much more significant than the solute diffusion mechanism.
3. A higher heat-extraction rate at the bottom of the casting increases the solidification rate, decreasing the size of the mushy zone, and lessens the severity of inverse segregation.
4. The predicted inverse segregation compared favorably with the published experimental data and the previous theoretical results using much simpler and restricted models.

NOMENCLATURE

c	specific heat
C	coefficient, defined in Eq. [9]
c_l	permeability coefficient, defined in Eq. [8]
d	dendrite arm spacing
D	mass-diffusion coefficient
f	mass fraction
g	volume fraction or gravitational acceleration
h	enthalpy
H	latent heat
k	thermal conductivity
k_p	equilibrium partition ratio
K	permeability
p	pressure
t	time
T	temperature
T_m	fusion temperature at zero solute concentration
u	velocity in the x-direction
v	velocity in the y-direction
$\mathbf{V}$	velocity vector
$\mathbf{V}_r$	relative velocity vector ($\mathbf{V}_l - \mathbf{V}_s$)
x, y	Cartesian coordinates

Greek Symbols

β_S	solutal expansion coefficient
β_T	thermal expansion coefficient
ε	rate of temperature change
μ	dynamic viscosity
ρ	density

Subscripts

0	initial value
c	chill
e	eutectic
l	liquid phase
m	fusion
r	relative to solid velocity
s	solid phase

Superscript

α	constituent of alloy

ACKNOWLEDGMENTS

The authors are grateful for the partial support by the Air Force Office of Scientific Research under Contract No. F49620-88-C-0053/SB5881-0378.

REFERENCES

1. M.C. Flemings: *Solidification Processing*, McGraw-Hill, Inc., New York, NY, 1974, pp. 214-58.
2. K.M. Fisher: *PCH, PhysicoChem. Hydrodyn.*, 1981, vol. 2, pp. 311-26.
3. E. Scheil: *Metallforschung*, 1947, vol. 2, pp. 69-75.
4. J.S. Kirkaldy and W.V. Youdelis: *Trans. TMS-AIME*, 1958, vol. 212, pp. 833-40.
5. M.C. Flemings and G.E. Nereo: *Trans. TMS-AIME*, 1967, vol. 239, pp. 1449-61.
6. M.C. Flemings, R. Mehrabian, and G.E. Nereo: *Trans. TMS-AIME*, 1968, vol. 242, pp. 41-49.
7. M.C. Flemings and G.E. Nereo: *Trans. TMS-AIME*, 1968, vol. 242, pp. 50-55.
8. H. Kato and J.R. Cahoon: *Metall. Trans. A*, 1985, vol. 16A, pp. 579-87.
9. I. Ohnaka and M. Matsumoto: *Tetsu-to-Hagané (J. Iron Steel Inst. Jpn.)*, 1987, vol. 73, pp. 1698-1705.
10. I. Ohnaka and M. Matsumoto: *Trans. Iron Steel Inst. Jpn.*, 1986, vol. 26, pp. 781-89.
11. W.D. Bennon and F.P. Incropera: *Int. J. Heat Mass Transfer*, 1987, vol. 30, pp. 2161-70.
12. W.D. Bennon and F.P. Incropera: *Int. J. Heat Mass Transfer*, 1987, vol. 30, pp. 2171-87.
13. C. Beckermann and R. Viskanta: *PCH, PhysicoChem. Hydrodyn.*, 1988, vol. 10, pp. 195-213.
14. D.G. Neilson and F.P. Incropera: *Int. J. Heat Mass Transfer*, 1991, vol. 34, pp. 1717-32.
15. K.C. Chiang and H.L. Tsai: *Int. J. Heat Mass Transfer*, 1992, vol. 35, pp. 1763-70.
16. K.C. Chiang and H.L. Tsai: *Int. J. Heat Mass Transfer*, 1992, vol. 35, pp. 1771-78.
17. P.C. Carman: *Trans. Inst. Chem. Eng.*, 1937, vol. 15, pp. 150-66.
18. K. Kubo and R.D. Pehlke: *Metall. Trans. B*, 1985, vol. 16B, pp. 359-66.
19. G.S. Beavers and E.M. Sparrow: *J. Appl. Mech.*, 1969, vol. 36, pp. 711-14.
20. J. Ni and C. Beckermann: *Transport Phenomena in Material Processing*, M. Charmichi, M.K. Chyu, Y. Joshi, and S.M. Walsh, eds., ASME HTD, Fairfield, NJ, 1990, vol. 32, pp. 45-56.

21. S.V. Patankar: *Numerical Heat Transfer and Fluid Flow*, Hemisphere. New York, NY, 1980, pp. 96-102.
22. K.C. Chiang: Ph.D. Thesis, University of Missouri–Rolla, Rolla, MO, 1990.
23. R.D. Pehlke, A. Jeyarajan, and H. Wada: *Summary of Thermal Properties for Casting Alloys and Mold Materials*, Report No. PB83-211003, National Technical Information Service, Washington, DC, 1983, pp. 81-93.